Scientia Iranica B (2022) 29(6), 3049–3062

Sharif University of Technology
**Scientia Iranica**
*Transactions B: Mechanical Engineering*
http://scientiairanica.sharif.edu

# Optimal design of flow mode semi-active prosthetic knee dampers

**R.S.T. Saini[a], H. Kumar[a,*], and S. Chandramohan[b]**

a. *Department of Mechanical Engineering, National Institute of Technology Karnataka, Surathkal–575025, India.*
b. *Department of Mechanical Engineering, Indian Institute of Technology Madras, Chennai–600036, India.*

Received 24 August 2021; received in revised form 14 March 2022; accepted 11 July 2022

**KEYWORDS**
Prosthetic knee;
Magnetorheological devices;
Twin-rod;
Rotary vane;
Limited angle motion;
Particle swarm optimization.

**Abstract.** Magnetorheological (MR) fluid devices operate in four modes: flow, shear, squeeze, and pinch. Among these, the flow mode is the most efficient one and results in large field-induced pressure differences. Despite being the least efficient, shear mode is the most commonly used in numerous applications, including prosthetic knees, due to its ease of construction. Additionally, shear mode designs require larger shear areas and reduced fluid gap tolerance compared to their flow mode counterparts, resulting in a complex design such as the commercially available multi-plate MR brake. Therefore, in this study, two flow mode designs, twin-rod and rotary vane MR dampers, are optimally designed for prosthetic knee application. The optimal designs obtained from solving a multi-objective particle swarm optimization problem are fabricated and experimentally characterized for various harmonic excitations of varying amplitudes, frequencies, and currents. The optimal designs are compared with many MR fluid-based prosthetic knee design configurations. Based on the results, a twin-rod MR damper with a mass of 0.71 kg and a damping force of 1020 N at 1 A is identified as the optimal design configuration for prosthetic knee application.



## 1. Introduction

A knee prosthesis is a device used to support transfemoral amputees in performing activities of daily life. While the use of compliant joints results in increased energy efficiency and lighter mechanisms, they cannot meet all of the functional needs of users [1]. On the other hand, semi-active prosthetic knee can provide variable damping and stand as a cheaper compromise between passive and active knees. This may be accomplished by the use of variable orifice dampers, smart fluids, and so on.

*. *Corresponding author. Tel.: (0824) 247 3681*
*E-mail addresses: sainiradhe06@gmail.com (R.S.T. Saini); hemantha@nitk.edu.in (H. Kumar); sujatha@iitm.ac.in (S. Chandramohan)*

doi: 10.24200/sci.2022.58926.5971

Magnetorheological (MR) fluid is a class of smart fluid that uses magnetic particles suspended in a base oil along with a few additives. When the magnetic field is applied, the particles align themselves in a reversible manner altering the rheology of the fluid [2]. Based on the fluid flow, geometry, and applied magnetic field direction, there are four distinct modes of operation: flow, shear, squeeze, and pinch, as shown in Figure 1. The flow mode is the most realized one, producing high field-induced pressure differences, whereas shear mode is the least efficient, requiring large shearing areas and tight fluid gap tolerance to generate desired loads. Squeeze mode is limited to low amplitude vibration applications, whereas the pinch mode is capable of generating pressure differences of magnitude greater than the other three modes, but has been identified more recently and requires extensive studies [3,4].

Many designs have been studied exploiting these fluid modes and various novel geometric configurations

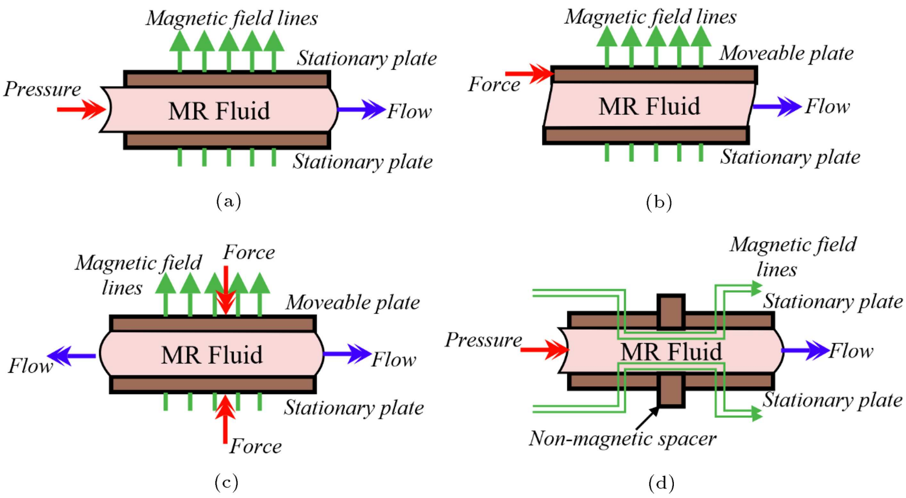


**Figure 1.** Working modes of operation of MR fluid.

and applications have been produced [4,5]. Incidentally, prosthetic knee devices are mostly shear mode based designs such as multi-plate brake [6], multi-pole brake [7], disc type [8], waveform boundary brake [9,10], and twin-rod shear damper [11,12]. Although linear flow mode dampers have been extensively studied for other applications, their usage in prosthetic knee devices is relatively scarce and is limited to few theoretical MR valve designs [13]. On the other hand, rotary MR damper design by Kim and Oh [14] is the only novel prosthetic knee damper working on flow mode configuration. However, the design can generate a maximum damping torque of 23 Nm, which is insufficient for a normal average human walking. Also, the rotary chamber used was a retrofit pneumatic component, which suggests an optimal design study. A few other studies performed on rotary vane dampers were only limited to theoretical designs with no experimental characterization [15,16]. Therefore, based on the previous studies, optimal design of two flow mode MR dampers (linear twin-rod and rotary vane) for prosthetic knee application is considered in this study.

Although many studies have been performed on design optimization of MR dampers, most of them have considered a lumped parametric Magnetic Equivalent Circuit (MEC) method, resulting in sub-optimal design solutions. Apart from the reported inaccuracies in magnetic field distribution in the model, MEC method does not provide any information about maximum core flux, which is an important constraint in design problems as it provides information about bottleneck of magnetic flux lines. Therefore, this study adopts a recently proposed optimization approach with comparable accuracy levels, which is one of the finite element methods and is computationally inexpensive in nature.

Furthermore, objective functions commonly used in optimal design studies of prosthetic knee dampers include on-state braking torque or force, off-state braking torque or force, and mass and power dissipation. As suggested by our previous research work, the use of mass and power dissipation as an objective function yields a redundant optimization problem as the reduction of the overall device mass eventually decreases the coil volume, which ultimately lowers power dissipation [17]. Moreover, amputee's mass proportionately increases the on-state braking torque requirements, while the off-state torques that primarily control the swing phase of gait cycle remain mostly unaffected. Therefore, in this study, on-state braking torque (or equivalent force) and mass are chosen as objectives while off-state braking torque (or equivalent force) maximum core flux are applied as constraints.

Based on the above objectives, the optimal designs of twin-rod and rotary vane dampers are implemented considering various shortcomings in the design methodologies of previous studies. The fabricated prototypes of the two devices are characterized by various harmonic inputs. Finally, the experimental results are compared with those from the previous studies and also with commercial prosthetic knee models.

## 2. Geometric modeling of twin rod MR damper

The schematic diagram of the prosthetic knee incorporated with twin-rod MR damper is shown in Figure 2. As seen in the figure, one end of the damper is connected to the thigh using an extensor link, whereas the other end is connected to the shank. The damper consists of a piston core assembly with piston rods on both ends enclosed in a cylinder. The piston core assembly is formed of inner and outer cores with an electromagnetic coil wound on the inner core. MR fluid flows through a small gap between the two cores and its rheological properties are altered using a controllable magnetic field in the gap. After initial

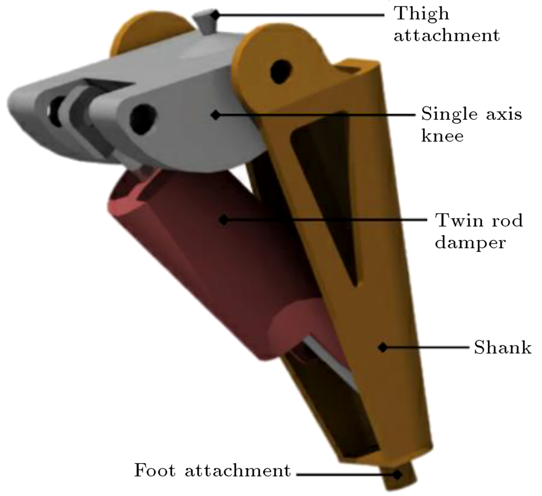


**Figure 2.** Schematic of prosthetic knee incorporated with twin-rod damper.

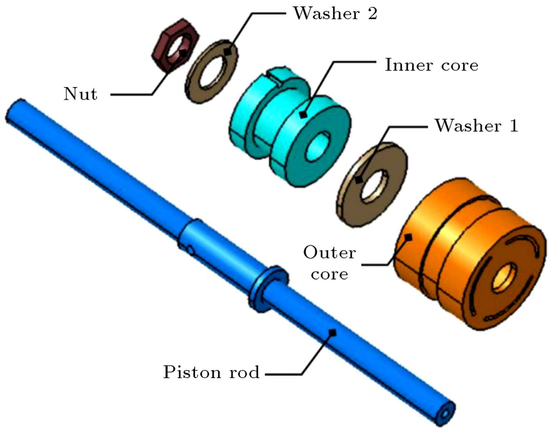


**Figure 3.** Piston core assembly.

prototyping and observations, the piston core assembly of the twin-rod MR damper is modified, as shown in Figure 3. The threaded joint on the stepped shaft holds the inner and outer cores together and prevents any fluid leakage from the piston through-hole. To avoid flux leakage due to direct contact between the cores, aluminium washers have been placed between them. The geometric variables of the twin-rod damper are shown in Figure 4.

The total damping force can be calculated using Eq. (1) [18]:

$$F_{Total} = \frac{12\eta Q L_t A_p}{w_t g^3} + \left[2.07 + \frac{12Q\eta}{12Q\eta + 0.4 w_t g^2 \tau_y}\right] \frac{\tau_y (2L_a) A_p}{g}. \quad (1)$$

Here, $w_t$ is the average circumference of fluid gap, $g$ the fluid gap, $Q$ the flow velocity, $A_p$ the piston cross-section area, $L_a$ the active pole length, $\eta$ the fluid

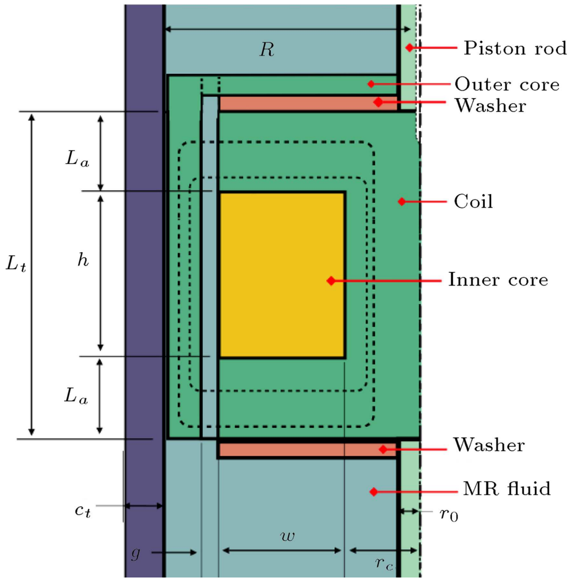


**Figure 4.** Geometrical variables of twin-rod MR damper.

viscosity, and $\tau_y$ the fluid yield stress. The first part of Eq. (1) represents the viscous force, $F_{vis}$, and the second part of the equation represents the controllable MR force, $F_{MR}$. A few of the dependent variables are given by Eqs. (2)–(4):

$$w_t = 2\pi(r_c + w + 0.5g), \quad (2)$$

$$A_p = \pi[R^2 - r_0^2], \quad (3)$$

$$Q = A_p \dot{u}. \quad (4)$$

Here, $r_0$ is the piston rod radius, $\dot{u}$ the velocity of piston and $r_c$ the radius of the MR valve core. The volumes of the coil, piston rod, MR fluid, inner core, and outer core in the piston core assembly are calculated using Eqs. (5)–(9):

$$V_{coil} = \pi\left[(r_c + w)^2 - r_c^2\right] h, \quad (5)$$

$$V_{rod} = \pi r_0^2 L_t, \quad (6)$$

$$V_{MRF} = \pi\left[(r_c + w + g)^2 - (r_c + w)^2\right] L_t, \quad (7)$$

$$V_{core} = \pi\left[(r_c + w)^2 - r_0^2\right] L_t - V_{coil}, \quad (8)$$

$$V_{outer\ core} = \pi\left[(r_c + w + g + c_t)^2 - (r_c + w + g)^2\right] L_t. \quad (9)$$

Here, $c_t$ is the outer cylinder thickness. The mass of the piston rod assembly is calculated using Eq. (10):

$$m_P = \rho_{coil} V_{coil} + \rho_{core}\left(V_{core} + V_{outer\ core} + V_{rod}\right) + \rho_{MRF} V_{MRF}. \quad (10)$$

Here, $\rho_{coil}$, $\rho_{core}$, and $\rho_{MRF}$ are the densities of the coil, core, and MR fluid materials, respectively. The overall mass of the twin-rod MR damper, $M$, is calculated assuming a cylinder cap thickness of 15 mm, piston rod radius of 4 mm, design velocity of 0.1 m/s, and a stroke length of 55 mm. Also, 1018 steel is selected as the core material due to its high magnetic permeability and low cost. The piston rod is assumed to be made of stainless steel and the outer cylinder is of mild steel. MRF-132 DG (Make: Lord Corporation) is selected as the MR fluid and the properties of the same are obtained from the datasheet [19]. A packing factor of 0.6 was considered while calculating the number of turns of the electromagnetic coil [20].

### *2.1. Optimal design of twin-rod MR damper*

An optimal design of the twin-rod MR damper is performed considering the total damping force and mass as the objectives. The design variables and bounds are shown in Table 1. These values are selected such that the damper can be enclosed within the shank volume of an average human. An optimization problem of the twin-rod MR damper is formulated as follows:

Objective function: Minimization of $[-F_{Total}, M]$,

Constraints: $M < 1$ kg, $B_{\max} < 1.8$ T and $F_{vis} < 80$ N.

The optimization is performed using Particle Swarm Optimization (PSO), an algorithm based on the movement of flock of birds. The population of design variable vector is updated using social and cognitive constants analogous to birds' motion and behavior. The objective functions and the constraints depend on the magnetic flux distribution in the axisymmetric model of the geometry, which is usually evaluated using Finite Element Modeling (FEM) or MEC methods. FEM methods produce accurate magnetic field distribution, but are computationally expensive. In spite of less accuracy, MEC methods have been widely used in previous studies due to their computationally inexpensive nature. However, to ensure better accuracy with low computational costs, a combined magnetostatic approach was proposed in our previous work [17]. This approach was found to produce accurate design solutions similar to FEM-based optimization and was also computationally less expensive. The methodology of the optimization problem is shown in Figure 5. As seen in the figure, the initial objective functions are evaluated using MEC method. The elite candidates are selected by lot and the cost functions are re-evaluated on the reduced population using FEM method. This approach is employed to reduce the number of FEM evaluations and thus, to increase the design solution accuracy and also reduce the computational time. The optimization problem is performed with a population of 50 and 100 iterations. The Pareto optimal front solutions of the twin-rod MR damper are shown in Figure 6.

**Table 1.** Variables, bounds, and optimized values of twin-rod MR damper.

| Variables | Bounds (mm) | | Optimized values (mm) |
|---|---|---|---|
| | Lower | Upper | |
| $r_c$ | 6 | 16 | 9.8 |
| $w$ | 2 | 10 | 3.4 |
| $h$ | 2 | 10 | 10 |
| $g$ | 0.5 | 1.2 | 0.67 |
| $L_a$ | 3 | 10 | 6 |
| $c_t$ | 3 | 10 | 3 |

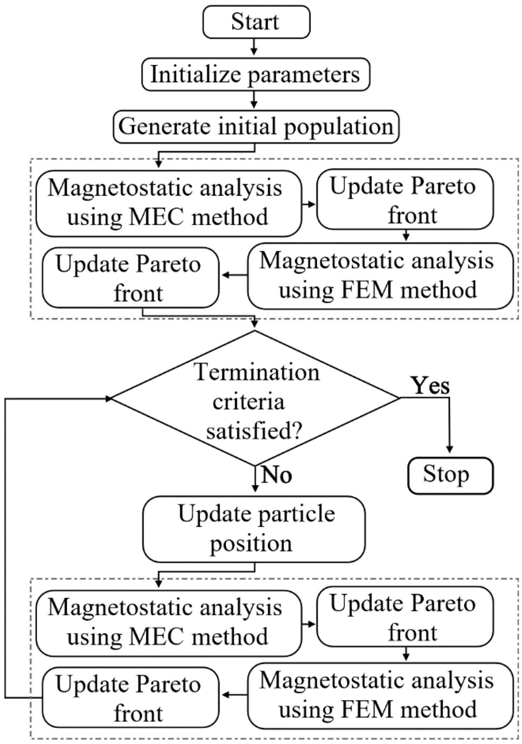


**Figure 5.** Optimization methodology.

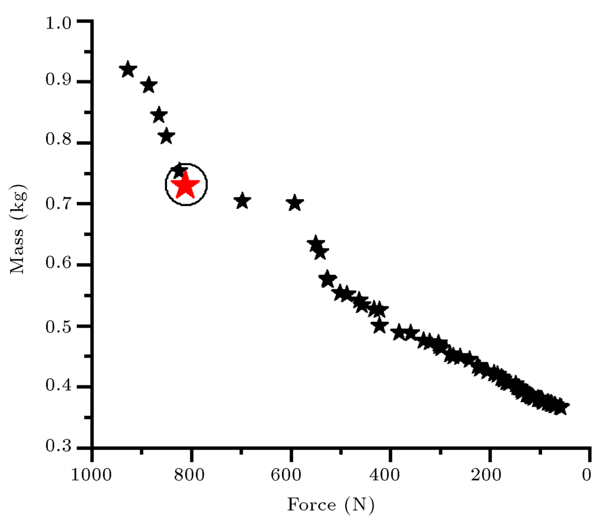


**Figure 6.** Pareto front of twin-rod MR damper.

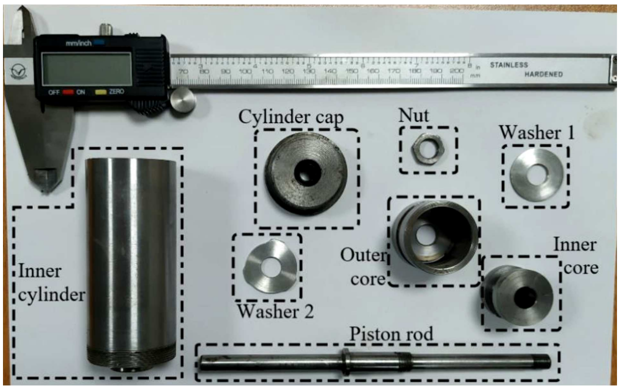


**Figure 7.** Fabricated components of twin-rod MR damper.

An average person of mass 56.7 kg has a maximum knee braking torque requirement of 35 Nm [21]. Considering a moment arm of 40 mm and based on the previously reported differences between theoretical and experimental damping force values, a cut-off of 800 N is assumed and the optimal solution with the least possible weight above this cut-off is selected. The optimal design point (colored in red in Figure 6) produces a damping force of 812 N with a mass of 0.73 kg. The dimensions of the optimal point are listed in Table 1. The fabricated components of the optimal twin-rod MR damper are shown in Figure 7.

### *2.2. Characterization of damper*

An in-house prepared MR fluid with 80.95% mass fraction of carbonyl iron particles similar to MRF-132DG is synthesized. The composition and characterization results of the fluid were reported in another study on optimal composition of MR fluids by our research group [22]. It was estimated that the in-house MR fluid yielded similar performance metrics to that of MRF-132DG and was, thus, used for damper characterization in this study. The MR fluid sample was de-gassed in a vacuum chamber prior to filling the twin-rod MR damper. The damper was characterized using a linear dynamic testing facility. A hydraulic actuator (Type: double acting, Capacity: +/−20 kN, Stroke:

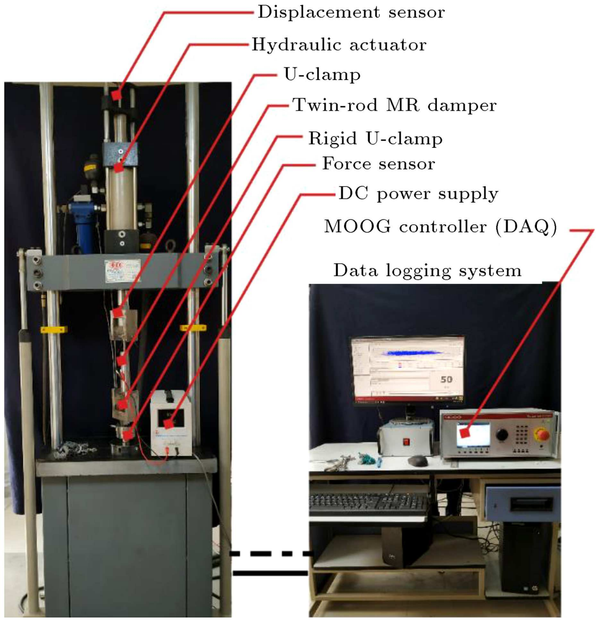


**Figure 8.** Linear dynamic testing machine.

150 mm) controlled by a servo valve provides the actuating force to the damper. A force transducer (Capacity: +/−30 kN and Resolution: 0.001 kN) at the rigid end and a displacement sensor (Make: Gefran, Range: 200 mm) at the actuator end measure the force and displacement signals, respectively. The signals are acquired using a data acquisition system (Make: MOOG) and stored for further processing. The test setup and the installed twin-rod MR damper are shown in Figure 8. The damper is tested for harmonic excitations of various amplitudes, frequencies, and currents. Sample characteristic curves showing the variation of force with displacement and velocities at varying currents are shown in Figure 9.

Theoretically, the optimal design of the twin-rod MR damper produces a damping force of around 812 N at a design speed of 0.1 m/s and at a current of 1 A. Off-state damping force of the damper is around 82 N. Based on the experimental results in Figure 9, the damper produces a total force of 1020 N at the same

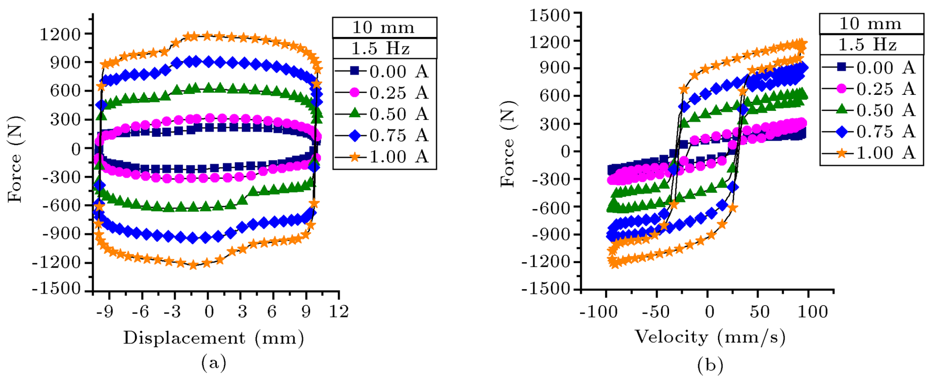


**Figure 9.** (a) Force-displacement and (b) force-velocity curves of linear twin-rod MR damper for varying currents.

design speed of 0.1 m/s and a current of 1 A. The off-state damping force at the same speed is found to be 135 N. Unaccounted friction due to wiper seals on both sides of piston rod along with slight manufacturing deviations might contribute to deviation in results. However, the increase of total damping force and the reduction of overall mass can be considered as positive indicators for this application.

## 3. Geometric modeling of rotary vane MR damper

The schematic of the prosthetic knee component incorporated with the rotary vane damper is shown in Figure 10. As seen in figure, the rotary vane damper itself acts as the knee joint with the MR bypass valve placed in the shank. Since the normal human knee rotary motions are limited to 130°, a semi-circular cross-section for vane damper can reduce the amount of MR fluid usage and the weight of the damper. However, to simplify prototype manufacturing, it is retained as circular with the other half packed using a static vane. The exploded view of the rotary vane damper and the MR valve is shown in Figure 11. The rotary chamber accommodates a fixed static vane and a rotary vane rotating with the shaft. The motion of the shaft drives the MR fluid from one chamber to another through hydraulic ports and cables. The fluid flows through the bypass MR valve which consists of an inner core and a valve cylinder realizing a flow mode configuration for the MR fluid. The geometric variables of vane type MR damper are shown in Figure 12.

The total damping torque produced by the vane damper is calculated using Eq. (11) [23]:

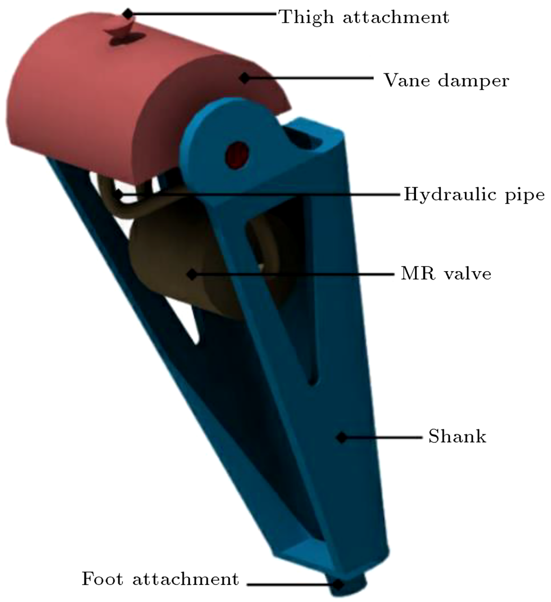


**Figure 10.** Semi-active prosthetic knee incorporated with rotary vane MR damper.

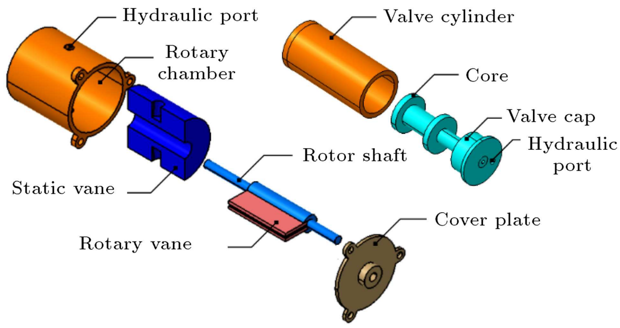


**Figure 11.** Exploded view of rotary vane MR damper.

$$T = \frac{12\eta Q L_t}{g^3 w}(L_r w_r R_r) + \left[\left(2.07 + \frac{12Q\eta}{12Q\eta + 0.4 w_t g^2 \tau_y}\right)\frac{2\tau_y L_a}{g}\right](L_r w_r R_r). \quad (11)$$

Here, $L_r$ is the height of the rotary vane in the axial direction along the shaft, $w_r$ the width of rotary vane along the radial direction, $R_r$ the radial distance from the shaft axis to the centroid of rotary vane, $w_t$ the average circumference of the MR flow channel, $w$ the width of the coil, $h$ the height of the coil, $g$ the fluid gap, and $L_a$ the pole length of MR valve. The first part of Eq. (11) represents the viscous or off-state damping torque, $T_{vis}$, and the second part of the equation represents the controllable damping torque, $T_{MR}$.

The average flow rate of the MR fluid and the radial distance can be calculated using the equations:

$$Q = L_r w_r R_r \omega, \quad (12)$$

$$R_r = R_0 + 0.5 w_r. \quad (13)$$

Here, $\omega$ is the design speed taken as 8.6 rpm and $R_0$ the radius of rotor shaft taken as 4 mm. Also, the parameters including cover plate thickness, rotor cylinder thickness, and MR valve thickness are set to 4 mm. These parameters are required to calculate the overall mass of the braking torque and are estimated based on the previous study [23]. The approximate volumes of coil, rod, MR fluid, inner core, outer core, and cap of MR valve are calculated using Eqs. (14)–(19):

$$V_{coil} = \pi\left[(r_c + w)^2 - r_c^2\right] h, \quad (14)$$

$$V_{rod} = 1.2\pi r_0^2 L_t, \quad (15)$$

$$V_{MRF} = \pi\left[(r_c + w + g)^2 - (r_c + w)^2\right] L_t + 0.4\pi L_t\left[(r_c + w + g)^2 - r_0^2\right], \quad (16)$$

$$V_{core} = \pi\left[(r_c + w)^2 - r_0^2\right] L_t - V_{coil}, \quad (17)$$

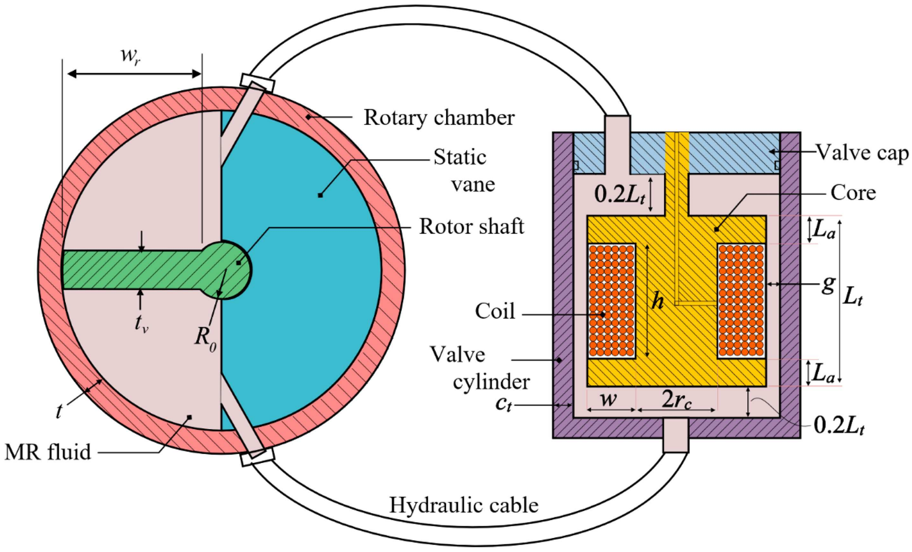


**Figure 12.** Geometric variables of rotary vane MR damper.

$$V_{outer\ core} = 1.4\pi L_t\left[(r_c+w+g+c_t)^2-(r_c+w+g)^2\right], \quad (18)$$

$$V_{cap} = \pi(r_c + w + g + c_t)^2 t_c. \quad (19)$$

The mass of the MR valve is calculated using Eq. (20):

$$m_{valve} = \rho_{coil}V_{coil} + \rho_{core}(V_{core} + V_{outer\ core} + V_{rod}+V_{cap})+\rho_{MRF}V_{MRF}+\rho_{Al} * V_{cap}. \quad (20)$$

Here, $\rho_{Al}$ is the density of aluminium. The core and cylinder are assumed to be made of 1018 steel and all other components are made of aluminium material. The mass of the rotary vane, MR fluid in the rotary chamber, and the rotary enclosure are calculated using Eqs. (21)–(23):

$$m_{RVane} = \rho_{Al}[\pi R_0^2(L_r + 2t) + L_r w_r t_v], \quad (21)$$

$$m_{RMRF} = \rho_{MRF}\{0.5\pi\left[(R_0 + w_r)^2 - R_0^2\right] - L_r w_r t_v\}, \quad (22)$$

$$m_{Renc} = \rho_{Al}\left(\pi L_r(R_0+w_r+t)^2 - (R_0+w_r)^2\right) + 2\pi t_c(R_0 + w_r + t)^2. \quad (23)$$

The overall mass of the rotary vane MR damper is calculated using Eq. (24):

$$m_{Total} = m_{valve} + m_{RVane} + m_{RMRF} + m_{Renc}. \quad (24)$$

### 3.1. Optimal design of rotary vane MR damper

An optimization problem of rotary vane MR damper is formulated as follows:

Objective function: Minimization of $[-T, m_{Total}]$,

Constraints: $m_{Total} < 1$ kg, $B_{\max} < 1.8$ T and $T_{vis} <$ 2.5 Nm.

The design variables and bounds listed in Table 2 are estimated so as to restrict the overall volume of the damper within the realizable size limits of normal human knee. The optimization problem is solved using PSO algorithm and the combined magnetostatic approach as detailed in the previous section. The Pareto optimal front showing various design points of rotary vane damper is shown in Figure 13.

The design point with a braking torque of more than 35 Nm and of least mass is selected as the optimal solution. The cut-off value is selected based on maximum knee braking torque of an average normal human. The optimal design is capable of producing a braking torque of around 37 Nm and has a total mass of around 0.8 kg. The optimal values of rotary vane damper are listed in Table 2. The mass of the static vane, hydraulic ports, and cables along with MR fluid occupying these components were not considered due to uncertainty. The fabricated components along with the hydraulic ports and cables are shown in Figure 14.

**Table 2.** Bounds and optimum values of design variables.

| Variables | Bounds Lower (mm) | Bounds Upper (mm) | Optimum values (mm) |
|---|---|---|---|
| $L_r$ | 40 | 80 | 65 |
| $w_r$ | 15 | 35 | 25 |
| $r_c$ | 5 | 14 | 9.8 |
| $w$ | 2 | 10 | 3 |
| $h$ | 2 | 10 | 10 |
| $g$ | 0.5 | 1.2 | 0.56 |
| $L_a$ | 3 | 10 | 8 |
| $c_t$ | 3 | 10 | 3.2 |

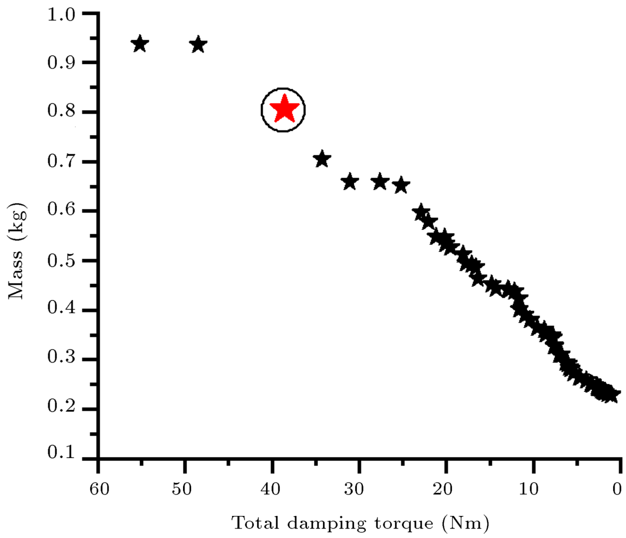


**Figure 13.** Pareto front of rotary vane MR damper.

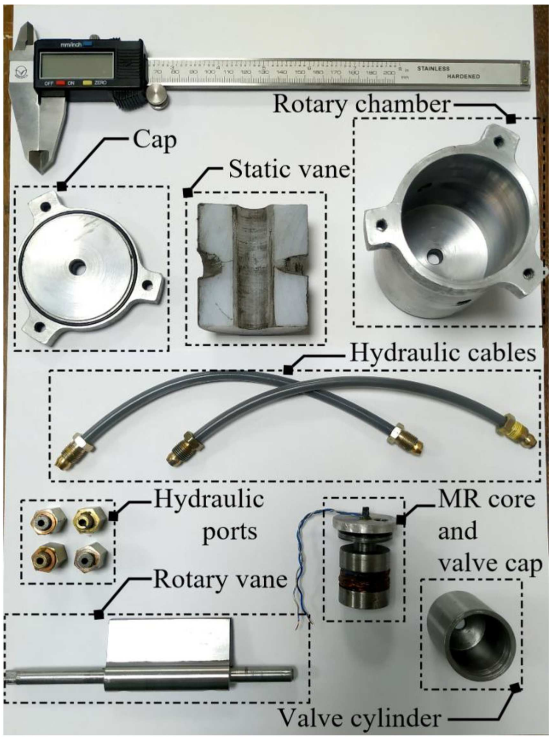


**Figure 14.** Fabricated components of rotary vane MR damper.

### *3.2. Characterization of damper*

A test facility to generate rotary harmonic excitations is developed to characterize the vane damper. The schematic of the rotary test setup is shown in Figure 15. A hybrid stepper motor (Make: Rhino Motions, Model: RMCS-1056) is used to provide the required angular displacements. A Leadshine servo drive (Model: ES-D1008) is adopted to drive the stepper motor. The motor was coupled with a planetary gear box (Gear ratio 10:1) to reduce the speed and increase the torque capacity of characterization setup. A torque transducer (Make: Datum Electronics; Model: M425) is coupled in line with the rotary system with one end connected to the gear box shaft. The other end of the transducer is connected to the rotary damper. Various sub-systems are interconnected using suitable flexible shaft couplers. An encoder (Make: Rhino Motions, Model: RMCS-5102) is connected at the far end of the rotary damper to measure angular displacement. Bearing block supports are provided in various places to support individual subsystems and, also, to effectively transfer the motion from the motor to the rotary damper.

The stepper motor system is actuated independently using a micro-controller. The rotary damper is supported using a fixture so as to constrain the relative motion of the outer cylinder of the rotary chamber. The torque sensor display unit provides an analog output signal in the range of 0 to 10 V. This signal is acquired using an analog input module (Make-National Instruments; Model-NI 9205) connected to the chassis (Make-National Instruments; Model-cDAQ 9174). The torque and encoder signals are acquired using a LabVIEW program, which allows continuous monitoring along with data logging for subsequent analysis. The fabricated setup along with the rotary vane MR damper is shown in Figure 16. Sequential installation of individual subsystems in the order of motor, gearbox, torque transducer, rotary vane damper, and encoder is performed and alignment issues are corrected carefully. A few characteristic curves of the vane damper showing torque variation with currents are shown in Figure 17.

According to the characteristic curves of Figure 17(a), the displacement amplitude is not constant for all the curves. In the experimental test setup, the stepper motor actuation system is not based on a closed-loop position tracking control. Thus, the high dissipation torque of the damper prevents the motor from carrying out additional time steps necessary to reach the desired amplitude. However, the variation of torque with current for a specific displacement and frequency is clearly visible from the figures. Theoretically, the optimal design of a rotary vane MR damper can produce a total damping torque of 37 Nm at a design speed of 8.6 rpm (or 0.9 rad/s or 51.6 deg/s) and at a current of 1 A. However, the actual damping torque measured using experiments at a similar design speed and current value was around 20 Nm. Although the device generated a maximum damping torque of around 33 Nm at a speed of 23.6 rpm and a current of 1 A. The off-state torque also increased from 1.07 Nm in simulation to 5 Nm in the experiment. Moreover, the mass of the device increased from 0.8 kg to 1.1 kg.

To explore the reasons for the deviation of on-state torque, magnetostatic analysis of the axisymmet-

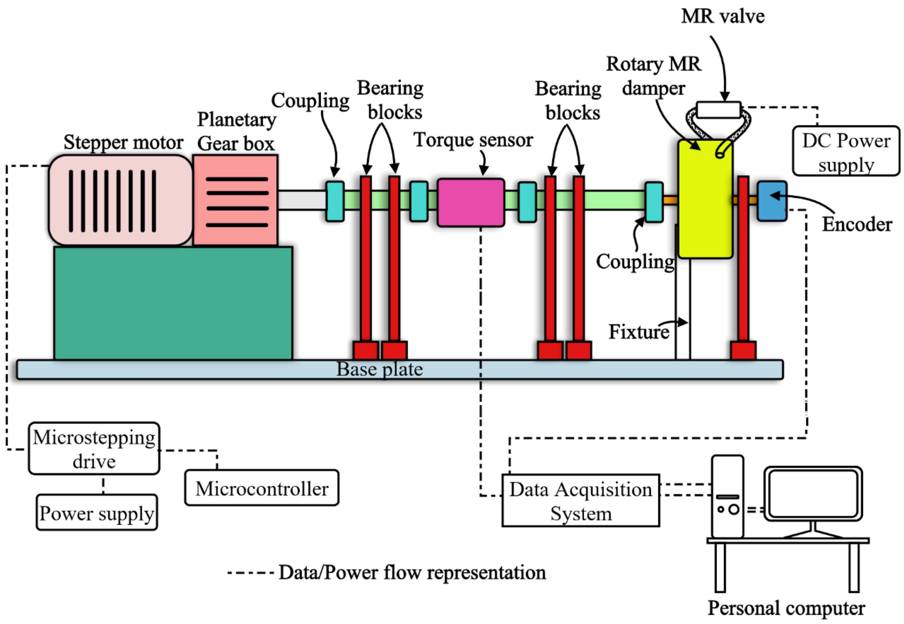


**Figure 15.** Schematic of rotary damper testing facility.

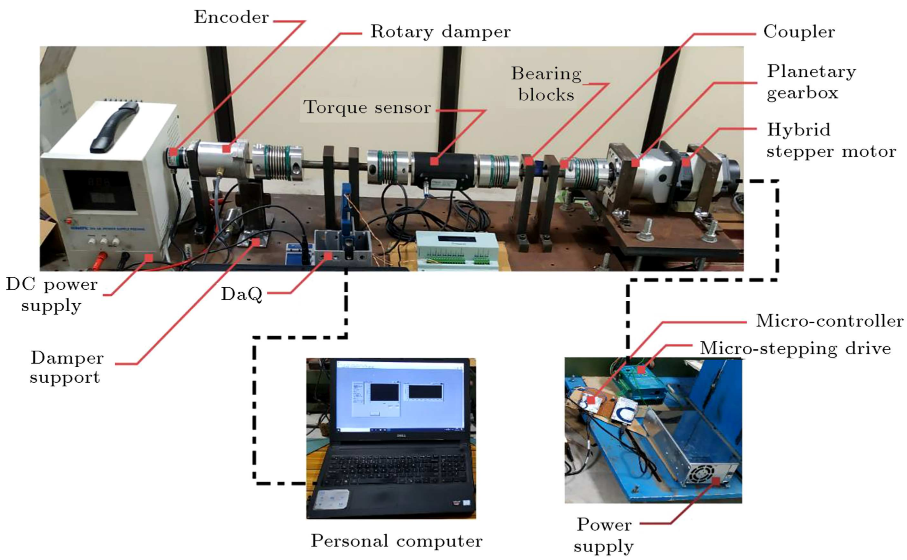


**Figure 16.** Rotary damper experimental test setup.

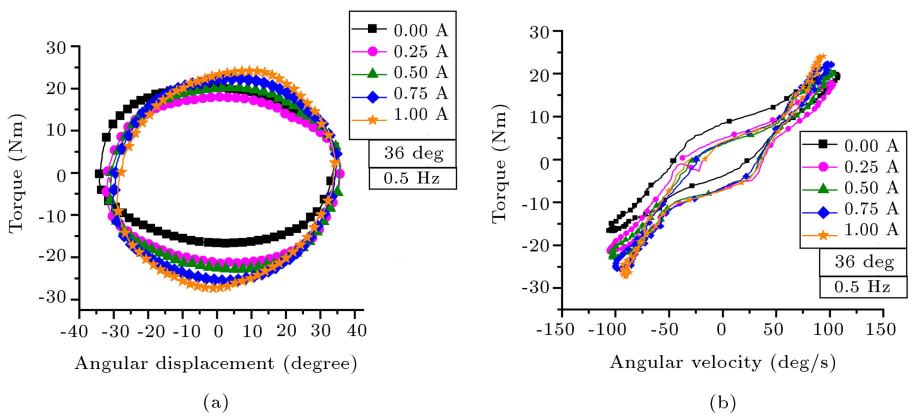


**Figure 17.** (a) Force-displacement and (b) force-velocity curves at 36-degree amplitude and 0.5 Hz frequency.

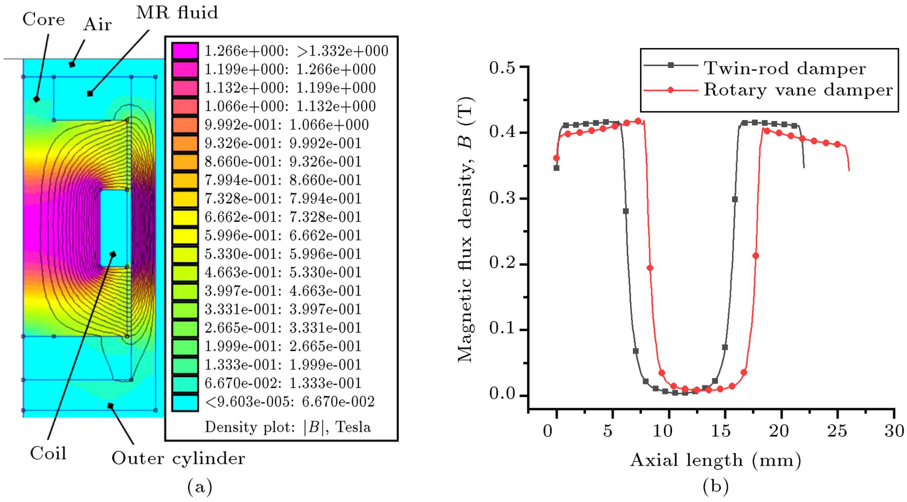


**Figure 18.** (a) Magnetostatic analysis of bypass MR valve and (b) magnetic flux density in fluid gap.

ric cross-section of the MR valve was performed using finite element method magnetics software [24]. This is an open-source finite element software product for solving 2D planar and axisymmetric problems in low-frequency magnetics and electrostatics. The model is discretized using triangular mesh with 4832 nodes. Figure 18(a) shows the magnetic field distribution in the MR valve. Further, the optimal twin-rod MR valve also produced a magnetic flux density distribution in the fluid gap similar to that of rotary vane MR valve, as evident from Figure 18(b). Moreover, other dimensional parameters and material properties are almost similar for both optimal designs, as can be verified from Tables 1 and 2. Since the performance of the MR valve in the twin-rod MR damper was in correlation with the theoretical design values, bypass MR valve can be safely neglected as a reason for obtaining a low dynamic range in the current design too. A few other possible reasons for the deviation between experimental and theoretical results are as follows:

1. Leakages around the axial or radial faces of the rotary vane and sides of static vane are considered as one of the main reasons for the underperformance of the design. Therefore, a low dynamic range of 1.4 was obtained due to the presence of leakage paths over high-resistance annular channels in the MR valve;
2. Use of multiple seals on rotary vane along with shaft seals, frictional losses due to multiple entrances and exits, and hydraulic losses contributed to the increase in off-state braking torque;
3. Unaccounted masses of hydraulic ports, cables, MR fluid, and static vane led to increase in the overall mass of device.

The rotary vane design by Kim and Oh [25] consists of a rectangular channel in a bypass MR valve, thus reducing many entrance and exit losses. This configuration resulted in an off-state torque of 1.5 Nm; however, the on-state torque was found insufficient for prosthetic knee application. Previous research on bypass MR valves (including those using linear MR damper configuration) assumed minimal losses owing to intricate valve dimensional changes. Although the dimensions of the hydraulic connections utilized in previous studies were not explicitly specified, they were noticeably larger than those employed in this investigation. The weight of the device is a significant restriction in this application; as a result, low-density hydraulic cables with an inner diameter of 4 mm were employed, which is believed to be one of the reasons for the large off-state damping torque. Similar differences in off-state damping forces were seen in a study by Idris et al. [26] who evaluated the use of a concentric bypass MR valve in conjunction with a linear damper. Off-state damping forces were found to be tenfold greater in experiments than in simulations identical to the current work. The researchers determined that the probable cause was seal friction. However, in comparison to the present bypass MR valve, the one developed by Idris et al. [26] is concentric in design and involves fewer valve dimensional changes, suggesting that frictional losses associated with these modifications might also possibly account for this difference.

It should be noted that the static vane can be completely avoided and the rotary chamber be made into a semi-circular cross-section. However, the additional mass due to hydraulic ports, cables, and MR fluids cannot be avoided. Since the vane damper design is the lowest possible mass design which can produce a required braking torque of more than 35 Nm, these additional units will further increase the mass of the vane damper even if they are specifically designed for this device. They also contribute to the increase of off-

**Table 3.** Comparison of prosthetic knee MR devices.

| Criteria | Current work | | Linear dampers | | | Rotary dampers/ MR brakes | | |
|---|---|---|---|---|---|---|---|---|
| | **Rotary damper** | **Linear damper** | **MR damper [11]** | **MR damper [30]** | **LORD RD-8040-1** | **Össur brake [9]** | **MR brake with waveform boundary [9]** | **Vane type MR damper [14]** |
| **Design** | Rotary vane type | Twin-rod damper | Twin-rod damper | Twin-rod damper | Mono tube | Multi plate | T-shaped rotor with waveform boundary | Rotary vane damper with MR valve |
| **Fluid regime** | Flow mode | Flow mode | Shear mode | Flow mode | Flow mode | Shear mode | Hybrid mode | Flow mode |
| **Mass (kg)** | 1.1 | **0.71** | 0.74 | - | 0.89 | 0.8 | 0.7 | — |
| **MR gap** | 0.56 mm | 0.67 mm | 1.1 mm | 1 mm | 0.2 −1 mm | 30 −35 $\mu$m | 0.2 mm | 1.4 mm |
| **Maximum on-state torque (Nm)** | 33@1 A | 40.8 Nm@1 A | 24@ 0.8 A | 6@90 mA | $\sim$ 48.9 Nm@1 A | 38 | 38.5@1.2 A | 23 |
| **Off-state torque (Nm)** | 5@8.6 rpm | $\sim$ 5.2 | 3.8 | 0.44 | $\sim$ 2.4 | 2.4@8 rpm | 2.1@5 rpm | 1.5 Nm@10 rpm |
| **Torque to mass ratio (Nm/kg)** | $\sim$ 30 | **57.46** | 32.43 | - | 54.94 | 47.5 | 55 | — |
| **Dynamic range** | 6.6 | 7.84 | 6.31 | 13.6 | 20.37 | 15.83 | 18.33 | 15.33 |

state braking torque. However, the device enjoys few advantages listed below:

1. The device can itself serve as a knee joint as opposed to the twin-rod MR damper, which requires a single-axis knee joint, along with an additional lever arrangement to convert a linear damping force into torque;
2. The weight of the vane damper acts mostly at the knee joint and, thus, does not add any additional moment of inertia to the prosthetic knee system. According to Narang et al. [27], the average hip power by the amputee is sensitive to the moment of inertia of the knee prosthetic system. Therefore, a reduced moment of inertia of the prosthetic knee may require lower hip energetics from the prosthetic user;
3. The placement of the MR valve unit may provide additional adjustment for the moment of inertia of the prosthetic knee system.

## 4. Comparative study

Table 3 shows a comparison of several dampers used in prosthetic knee systems with two damper designs developed in this work. To convert dynamic force into knee torque, a force arm length of 40 mm was used. As can be seen, the twin-rod MR damper is capable of providing the required braking torque at the knee joint and has higher performance indices than the commercial MR brake. It, however, has certainly a greater off-state braking torque. It should be noted that in the case of linear damper, the off-state force was computed at a design speed of 0.1 m/s. With an assumed arm length of 40 mm, this corresponds to a rotating speed of 2.5 rad/s, whereas the design speed of rotary brakes is around 0.84 rad/s (8 rpm). Given that the viscous force of a linear damper changes proportionately into the velocity, a reduced off-state damping force may be predicted at lower speeds. Additionally, it is expected that using a piston rod coating comparable to that utilized in commercial designs may further reduce the off-state damping force.

The mass of the twin-rod damper is less than that of all other devices fit for prosthetic applications, apart from the hybrid waveform boundary MR brake. The low dynamic range of the damper results from the high off-state force of the MR damper. Furthermore, the rotary vane damper in the current work outperforms the vane damper designed in the study by Kim and

Oh [14] in terms of on-state braking torque. However, it does not generate the required knee braking torque and, also, has a relatively high weight in comparison with other dampers fit for prosthetic knee applications. The vane damper requires many modifications in terms of design before it can be considered for prosthetic knee application. For instance, elimination of static vane and modification of MR valve design into a concentric flow type design are few of the suggested changes.

Another factor affecting the prosthetic knee damper design is the degree of deterioration of the MR fluid. This can be evaluated based on an ad-hoc measure and Lifetime Dissipated Energy (LDE) given by the following equation [28]:

$$LDE = \frac{1}{V}\int_0^{life} Pdt. \tag{25}$$

Here, $V$ is the volume of the MR fluid in the device and $P$ is the instantaneous mechanical power converted to heat. Assuming equal mechanical power during single walking cycle for all designs, LDE measure is thus scaled based on the volume of MR fluid, which is around 1.2 ml for commercial brake model and around 60 ml for current twin-rod MR damper. As a result, the twin-rod damper is expected to produce significantly lower LDE values for similar cycles.

The linear damper in the present work has a fluid gap tolerance of 0.67 mm as opposed to 30–35 $\mu$m for Össur brake. This allows the use of larger-sized iron particles reducing the overall cost of MR fluid. Moreover, larger fluid gap clearances allow for lower shear rates which, in turn, reduce MR fluid degradation [29]. Therefore, considering the present design configurations, it can be stated that the twin-rod MR damper from the current work can sufficiently produce the necessary damping force required during normal human walking, and it also is an optimal design for prosthetic knee application. Further experiments on the twin-rod MR damper are required to comment on durability, structural stability, and other aspects of overall prosthetic knee system integrated with the damper from the present work.

## 5. Conclusions

In the present work, two semi-active design configurations, i.e., twin-rod Magnetorheological (MR) damper and the rotary vane MR damper, were considered to be applied to prosthetic knee. Optimal designs were performed for both dampers with damping force or equivalent torque and mass as the objectives. In addition, core saturation and off-state force or torque were imposed as constraints. A constrained particle swarm optimization with a combined magnetostatic approach was used in the optimization process. The designs were fabricated and characterized using various harmonic excitations with varying amplitudes, frequencies, and currents. Based on the comparative study, it can be concluded that the twin-rod MR damper from the present work was an optimal design for prosthetic knee application, which could adequately reproduce the required knee damping forces. On the other hand, rotary dampers were previously designed for automotive applications with a torque generating capacity of 200 Nm. However, scaling of this product for prosthetic knee application led to large off-state torques along with a relatively large mass, resulting from sealing, intricate dimensional changes, and MR fluid viscosity. Consequently, it is suggested that concentric or in-pass MR valve designs be explored.

## Acknowledgements

The research was jointly supported by IMPRINT Project (Project no. IMPRINT/2016/7330), which is sponsored by Ministry of Human Resource Development and Ministry of Road Transport and Highways, Govt. of India and SPARC Project (Project no. 785) sponsored by Ministry of Human Resource Development, Govt. of India. The authors declare that the mentioned funding did not lead to any conflict of interests regarding the publication of this manuscript.

## Nomenclature

| | |
|---|---|
| $w_t$ | Average circumference of fluid gap |
| $g$ | Fluid gap |
| $Q$ | Flow velocity |
| $A_p$ | Piston cross-section area |
| $L_a$ | Active pole length |
| $w$ | Coil width |
| $h$ | Coil height |
| $\eta$ | Fluid viscosity |
| $\tau_y$ | Fluid yield stress |
| $F_{vis}$ | Viscous force |
| $F_{MR}$ | Controllable MR force |
| $F_{Total}$ | Total damping force |
| $r_0$ | Piston rod radius |
| $\dot{u}$ | Velocity of piston |
| $\rho$ | Density of material |
| $B_{\max}$ | Maximum flux density |
| $L_r$ | Height of rotary vane |
| $w_r$ | Width of rotary vane along radial direction |
| $R_r$ | Radial distance from shaft axis to centroid of rotary vane |

| | |
|---|---|
| $r_c$ | Radius of MR valve core |
| $w_t$ | Average circumference of MR flow channel |
| $c_t$ | Outer cylinder thickness |
| $\omega$ | Design speed |
| $R_0$ | Rotor shaft |
| $T$ | Total braking torque |
| $T_{vis}$ | Viscous torque |
| $T_{MR}$ | Controllable torque |

## References


1. Ghaemi, N., Zohoor, H., and Ghaemi, H. "Dynamic performance of different knee mechanisms with compliant joints", *Sci. Iran.*, **23**(3), pp. 1055–1063 (2016).
2. Carlson, J.D. "What makes a good MR fluid?", *J. Intell. Mater. Syst. Struct.*, **13**(7–8), pp. 431–435 (2002).
3. Goncalves, F.D. and Carlson, J.D. "An alternate operation mode for MR fluids-magnetic gradient pinch", *J. Phys. Conf. Ser.*, **149**, p. 012050 (2009).
4. Goldasz, J. and Sapiński, B., *Insight into Magnetorheological Shock Absorbers*, Springer International Publishing, Cham (2015).
5. Pourzeynali, S., Bahar, A., and Pourzeynali, S. "Vertical vibration control of suspension bridges subjected to earthquake by semi-active MR dampers", *Sci. Iran.*, **24**(2), pp. 439–451 (2017).
6. Andrade, R.M., Filho, A.B., Vimieiro, C.B.S., et al. "Optimal design and torque control of an active magnetorheological prosthetic knee", *Smart Mater. Struct.*, **27**(10), p. 105031 (2018).
7. Saini, R.S.T., Kumar, H., Chandramohan, S., et al. "Optimal design of rotary magneto-rheological drum brake for transfemoral prosthesis", *Lect. Notes Mech. Eng.*, pp. 465–474 (2021).
8. Arteaga, O., Terán, H.C., Morales, V., et al. "Design of human knee smart prosthesis with active torque control", *Int. J. Mech. Eng. Robot. Res.*, **9**(3), pp. 347–352 (2020).
9. Mousavi, S.H. and Sayyaadi, H. "Optimization and testing of a new prototype hybrid MR brake with arc form surface as a prosthetic knee", *IEEE/ASME Trans. Mechatronics*, **23**(3), pp. 1204–1214 (2018).
10. Sayyaadi, H. and Zareh, S.H. "Intelligent control of an MR prosthesis knee using of a hybrid self-organizing fuzzy controller and multidimensional wavelet NN", *J. Mech. Sci. Technol.*, **31**(7), pp. 3509–3518 (2017).
11. Gao, F., Liu, Y.N., and Liao, W.H. "Optimal design of a magnetorheological damper used in smart prosthetic knees", *Smart Mater. Struct.*, **26**(3), p. 035034 (2017).
12. Fu, Q., Wang, D.-H., Xu, L., et al. "A magnetorheological damper-based prosthetic knee (MRPK) and sliding mode tracking control method for an MRPK-based lower limb prosthesis", *Smart Mater. Struct.*, **26**(4), p. 045030 (2017).
13. Seid, S., Chandramohan, S., and Sujatha, S. "Optimal design of an MR damper valve for prosthetic knee application", *J. Mech. Sci. Technol.*, **32**(6), pp. 2959–2965 (2018).
14. Kim, J.H. and Oh, J.H. "Design and analysis of rotary MR damper using permanent magnet", *IFAC Proc.*, **35**(2), pp. 823–827 (2002).
15. Imaduddin, F., Mazlan, S.A., Zamzuri, H., et al. "By-pass rotary magnetorheological damper for automotive applications", *Appl. Mech. Mater.*, **663**, pp. 685–689 (2014).
16. Zhang, J.Q., Feng, Z.Z., and Jing, Q. "Optimization analysis of a new vane MRF damper", *J. Phys. Conf. Ser.*, **149**, p. 012087 (2009).
17. Saini, R.S.T., Kumar, H., and Chandramohan, S. "Optimal design of inverted rotary MR brake with waveform boundary using a novel combined magnetostatic approach", *Smart Mater. Struct.*, **29**(10), p. 105014 (2020).
18. Yang, G., Spencer, B.F., Carlson, J.D., et al. "Large-scale MR fluid dampers: Modeling and dynamic performance considerations", *Eng. Struct.*, **24**(3), pp. 309–323 (2002).
19. Lord Corporation, MRF-132DG Magneto-Rheological Fluid (2011).
20. Saini, R.S.T., Kumar, H., Chandramohan, S., et al. "Design of twin-rod flow mode magneto rheological damper for prosthetic knee application", *AIP Conf. Proc.* (2019).
21. Winter, D.A., *Biomechanics and Motor Control of Human Movement*, John Wiley & Sons, Inc., Hoboken, NJ, USA (2009).
22. Acharya, S., Saini, T.R.S., Sundaram, V., et al. "Selection of optimal composition of MR fluid for a brake designed using MOGA optimization coupled with magnetic FEA analysis", *J. Intell. Mater. Syst. Struct.*, **32**(16), pp. 1831-1854 (2020).
23. Saini, R.S.T., Chandramohan, S., Sujatha, S., et al. "Design of bypass rotary vane magnetorheological damper for prosthetic knee application", *J. Intell. Mater. Syst. Struct.*, **32**(9),pp. 931-942 (2020).
24. Meeker, D., *Finite Element Method Magnetics: OctaveFEMM User' s Manual*, pp. 1–59 (2010). http://www.femm.info/Archives/doc/octavefemm.pdf"
25. Kim, J.H. and Oh, J.H. "Development of an above knee prosthesis using MR damper and leg simulator", *Proc.-IEEE Int. Conf. Robot. Autom.*, **4**, pp. 3686–3691 (2001).
26. Idris, M.H., Imaduddin, F., Ubaidillah, Mazlan, S.A., et al. "A concentric design of a bypass magnetorheological fluid damper with a serpentine flux valve", *Actuators*, **9**(1), pp. 1–21 (2020).

27. Narang, Y.S., Arelekatti, V.N.M., and Winter, A.G. "The effects of prosthesis inertial properties on prosthetic knee moment and hip energetics required to achieve Able-Bodied kinematics", *IEEE Trans. Neural Syst. Rehabil. Eng.*, **24**(7), pp. 754–763 (2016).

28. Carlson, J.D. "MR fluids and devices in the real world", *Int. J. Mod. Phys. B*, **19**(7–9), pp. 1463–1470 (2005).

29. Hreinsson, E., *Durability of a Magnetorheological Fluid in a Prosthetic Knee Joint*, University of Iceland (2011).

30. Park, J., Yoon, G.H., Kang, J.W., et al. "Design and control of a prosthetic leg for above-knee amputees operated in semi-active and active modes", *Smart Mater. Struct.*, **25**(8), pp. 1–13 (2016).

## Biographies

**Radhe Shyam Tak Saini** received his PhD degree in Mechanical Engineering from National Institute of Technology, Surathkal, India in 2021. His dissertation focused on design and development of optimal magnetorheological dampers for prosthetic knee application. From 2017 to 2021, he worked as a research fellow at NITK Surathkal, working on design and development of semi-active devices for vehicular and prosthetic applications. His research interests include optimization, biomechanics, and smart material applications.

**Hemantha Kumar** received his BE degree from Mysore University in 2000, ME degree from Visvesvaraya Technological University in 2003, and PhD degree in Mechanical Engineering from Indian Institute of Technology Madras, Chennai, India in 2009. He is currently working as an Assistant Professor at Mechanical Engineering Department at National Institute of Technology Karnataka. He has led various research projects, supervised 10 PhD theses, and published more than 40 research articles in peer reviewed journals. His current research interests include vehicular dynamics and vibrations, condition monitoring, and smart fluids and its applications.

**Sujatha Chandramohan** received her BSc degree from Kerala University, India in 1979, MSc degree in Electrical engineering from Indian Institute of Technology Madras in 1987, and PhD degree in Applied Mechanical from IIT Madras in 1991. In 1981, she was with Indian Space Research Organization, Kerala, India as an engineer. She joined IIT Madras as a lecturer in 1992 and, thereafter, served the institute at various levels. She is currently working as a Professor at Mechanical Engineering Department at IIT Madras. She has published two books on vibration, acoustics, and signal processing, supervised more than 13 PhD theses, and co-authored more than 100 publications in peer-reviewed journals. Her current research interests include vibration and vehicle dynamics, smart fluids and applications, condition monitoring, signal analysis, and acoustics.